Characterizing the entanglement of symmetric many-particle spin-$\frac{1}{2}$ systems

John K. Stockton,* J. M. Geremia,† Andrew C. Doherty, and Hideo Mabuchi
Norman Bridge Laboratory of Physics 12-33, California Institute of Technology, Pasadena, California 91125
(Received 21 October 2002; published 28 February 2003)

Analyzing the properties of entanglement in many-particle spin-1/2 systems is generally difficult because the system's Hilbert space grows exponentially with the number of constituent particles, *N*. Fortunately, it is still possible to investigate a many-particle entanglement when the state of the system possesses sufficient symmetry. In this paper, we present a practical method for efficiently computing various bipartite entanglement measures for states in the symmetric subspace and perform these calculations for $N\sim 10^3$. By considering all possible bipartite splits, we construct a picture of the multiscale entanglement in large symmetric systems. In particular, we characterize dynamically generated spin-squeezed states by comparing them to known reference states (e.g., Greenberger-Horne-Zeilinger and Dicke states), and families of states with near-maximal bipartite entropy. We quantify the trade-off between the degree of entanglement and its robustness to particle loss, emphasizing that substantial entanglement need not be fragile.

DOI: 10.1103/PhysRevA.67.022112 PACS number(s): 03.65.Ud, 03.65.Db

I. INTRODUCTION

The structure of entanglement within multipartite quantum systems is a deep subject that has only begun to be explored. Since an ensemble's Hilbert space grows exponentially with the number of particles that comprise it, the number of distinct ways in which these particles can become entangled and the number of reference states needed to represent the various entanglement structures are immense [1]. While exponential scaling in complexity is the reason that multipartite entanglement is so rich, it is also the reason that the subject is so daunting.

Nonetheless, there is a motivation for characterizing entanglement in many-particle systems such as atomic spin ensembles because of recent experimental progress in creating and manipulating macroscopic quantum states. In particular, highly correlated atomic ensembles, such as spin-squeezed states [2], have been demonstrated [3–5] and advances are promised in atomic interferometry [6] and quantum communication [7]. They also provide experimentally accessible systems for studying quantum measurement, feedback, and control [8].

Spin squeezing is intimately linked to the structure of the entanglement between individual members of the ensemble [9,10]. However, without a complete microscopic picture of this entanglement, only limited claims about the structure of these correlated states can be made. In certain cases, an *N*-spin system can be characterized as either entangled or separable by measuring (computing) expectation values of total ensemble operators [11,12]. For example, if the spin-squeezing parameter for an *N*-spin state (with polarization along *z* and minimal variance along *x*) is less than unity,

$$\frac{N\langle J_x^2\rangle}{\langle J_z\rangle^2}<1, \tag{1}$$

then the state is guaranteed to be inseparable. However, at this level, limited information (in detail) about internal entanglement and its robustness to particle loss [13,14], or other types of decoherence [9,15,16], is available. In other words, entanglement tests using total ensemble operators cannot completely characterize the trade-off between the available entanglement resources and the state's fragility.

Unlike several multipartite techniques that have been introduced (e.g., the *N-tangle* [17]), we approach the problem of analyzing the *N*-particle entanglement using only bipartite measures. Although a single bipartite split of a large system is rarely sufficient to characterize multiparticle entanglement, combining the results from many different splits of the system paints a reconstructed picture of the many-particle entanglement. Furthermore, by repeating the analysis after removing particles from the system, it is possible to systematically characterize the entanglement across all size scales and its robustness to particle loss. Our approach has the advantage that it relies upon well-defined entanglement measures that are both computable and physically motivated.

Since substantial insight, and often a good starting point for more rigorous analysis, can be gained from numerical simulations, an efficient way of calculating entanglement measures is desirable. Section III develops the necessary machinery for calculating these measures in the symmetric subspace—the set of those *N*-particle pure states that remain unchanged by permutations of individual particles [10,18,19]. The main result of this section is that it is possible to perform partial transposes, partial traces, and Schmidt decompositions of symmetric states without resorting to an exponentially large representation of the system.

In Sec. IV, we characterize microscopic entanglement and its robustness to particle loss for several representative symmetric states, including the Greenberger-Horne-Zeilinger (GHZ) and Dicke (e.g., *W*) states. Here, the advantage of exploiting symmetry is clear; we perform entanglement calculations for systems with $N\sim 10^3$. These numerical results allow us to speculate on the large-*N* asymptotic scaling of the above entanglement measures. In some cases, particularly for the entanglement of formation and the reduced en-

*Electronic address: jks@Caltech.EDU
†Electronic address: jgeremia@Caltech.EDU

tropy, we analytically verify the observed scaling. We also introduce a family of states that provides insight into the scaling of bipartite entanglement in symmetric states for large N.

With the context provided by the reference states and the boundaries of allowed entanglement structures, we can better understand the entanglement generation abilities of certain dynamical processes. Section V focuses on the entanglement produced by spin-squeezing Hamiltonians. We illustrate the intuitive and generic effect that small-scale correlations peak before (and transform into) large-scale correlations. Again, the ability to simulate systems with $N \gg 1$ permits us to determine asymptotic behavior, both for large numbers of particles and for long times.

A point we stress is that *significantly entangled states need not be fragile*. Robustness is critically important in experiments, where the system constantly exchanges atoms with the surrounding environment. Moreover, we show that spin-squeezed states provide a reasonable compromise in this trade-off; they are highly entangled, yet particularly robust.

II. ENTANGLEMENT MEASURES

In this section, we review several common entanglement measures as motivation for the symmetric state techniques that are developed in Sec. III. In addition to recognizing the specific operations necessary for computing these entanglement quantities, we also describe their strengths, weaknesses, and, where possible, physical motivation.

We begin by reviewing the commonly accepted set of properties that all the measures of entanglement should share. For a general density matrix ρ, which can be divided into two or more subsystems, the quantity $E_X(\rho)$ (the label X is used to denote a generic measure) qualifies as an *entanglement monotone* if it satisfies the following conditions [20–22].

(C1) $E_X(\rho) \geqslant 0$; $E_X(\rho)=0$ if ρ is separable; $E_X(\text{Bell state})=1$.

(C2) Local operations classical communication (LOCC) and postselection do not increase $E_X(\rho)$ on an average. For example, with any state ρ, and partition $\{A,B\}$, local unitary transformations, $\hat{U}=\hat{U}_A \otimes \hat{U}_B$, do not affect $E_X(\rho)$.

(C3) Entanglement is convex under discarding information, $\Sigma_i p_i E_X(\rho_i) \geqslant E_X(\Sigma_i p_i \rho_i)$. We define the generalized Bell states as

$$|\Psi^{\pm}\rangle = (|1_A 0_B\rangle \pm |0_A 1_B\rangle)/\sqrt{2}, \tag{2}$$

$$|\Phi^{\pm}\rangle = (|1_A 1_B\rangle \pm |0_A 0_B\rangle)/\sqrt{2} \tag{3}$$

for a partition $\{A,B\}$ [52]. If the subsystem A has more than one spin, 1_A is interpreted as $1_1 \cdots 1_{N_A}$ and similarly for 1_B, 0_A, and 0_B.

A. Entropy of entanglement

Given a pure state $|\Psi\rangle$, and a partition for the system, $\{A,B\}$, the entropy of entanglement is defined as

$$E(|\Psi\rangle,\{A,B\}) \equiv S(\rho_A) = S(\rho_B), \tag{4}$$

where the von Neumann entropy is $S(\rho) = -\text{Tr}(\rho \log_2 \rho)$ and $\rho_A = \text{Tr}_B(|\Psi\rangle\langle\Psi|)$. Any entropy that results from performing a partial trace on the system must be a consequence of initial entanglement provided that the initial state is pure. For product states, $|\Psi\rangle = |\Psi\rangle_A \otimes |\Psi\rangle_B$, the entropy is zero since the single eigenvalue for each of the pure states ρ_A and ρ_B is one. The maximum entropy of entanglement gives a partition with dimensions, $\dim(A)=d_A$ and $\dim(B)=d_B$, with $d_A \leqslant d_B$, is $\log_2(d_A)$. A state that achieves this maximum is

$$|\Psi\rangle = |0\rangle_A \otimes |0\rangle_B + |1\rangle_A \otimes |1\rangle_B + \cdots + |d_A-1\rangle_A \otimes |d_A-1\rangle_B. \tag{5}$$

The entropy of entanglement has an interesting feature that it is straightforward to compute; it requires only performing a partial trace, $\rho_A = \text{Tr}_B(\rho)$, then computing eigenvalues of the result. The drawback of the entropy is that it only qualifies as an entanglement monotone for initially pure states.

B. Entanglement of formation

The entanglement of formation [23] is defined as

$$E_F(\rho,\{A,B\}) \equiv \min_{\{p_i,\psi_i\}} \sum_i p_i E(|\psi_i\rangle,\{A,B\}), \tag{6}$$

where $\{p_i,\psi_i\}$ satisfy the condition that $\rho = \Sigma_i p_i |\psi_i\rangle\langle\psi_i|$. This quantity is difficult to compute for mixed states but reduces to the entropy of entanglement for pure states.

In the special case of a mixed state of two spin-1/2 particles, the entanglement of formation can be computed from the two-particle concurrence, $\mathcal{C}(\rho)$ [23,24]. Therefore, it is generally possible to compute the entanglement of formation between two spins $\{i,j\}$ removed from an N-spin state $|\Psi\rangle$. The entanglement of formation for such a reduced system is a strong measure of the robustness of that state's entanglement to particle loss. Explicitly, for the two-particle state $\rho = \text{Tr}_{k \neq i,j} |\Psi\rangle\langle\Psi|$,

$$E_F(\rho,\{i,j\}) = h(\tfrac{1}{2}[1+\sqrt{1-\mathcal{C}(\rho)^2}]), \tag{7}$$

where $h(x) = -x \log_2(x) - (1-x)\log_2(1-x)$ and

$$\mathcal{C}(\rho) \equiv \max(0, \sqrt{\lambda_1} - \sqrt{\lambda_2} - \sqrt{\lambda_3} - \sqrt{\lambda_4}), \tag{8}$$

in which $\lambda_1, \ldots, \lambda_4$ are the eigenvalues of $\rho(\sigma_y \otimes \sigma_y)\rho^*(\sigma_y \otimes \sigma_y)$ in decreasing order and σ_y is a Pauli spin matrix.

C. Distillable entanglement and negativity

Given a mixed state ρ, and a partition $\{A,B\}$, the entanglement of distillation is defined as

$$E_D(\rho,\{A,B\}) \equiv \lim_{n \to \infty} \frac{m}{n}, \tag{9}$$

where m is the number of Bell states that can be distilled from n copies of ρ via an optimal purification protocol with LOCC [25,26]. For simplicity, we consider only the symmetric Bell state $|\Phi^+\rangle$ of Eq. (3) as the output of the distillation process throughout this paper. This state is also known as an Einstein-Podolsky-Rosen (EPR) pair, a GHZ state, or an N-particle cat (macroscopic quantum interference) state. The distillable entanglement is effectively a conversion efficiency; however, since the purification protocol allows auxiliary separable states to be introduced into the original system, it is possible, on an average, to extract more than one EPR pair from an initially entangled state. The distillable entanglement for an EPR pair is one by definition.

The advantages of the distillable entanglement are that it is a monotone for mixed initial states and that it quantifies entanglement as a practical resource. In this sense, the distillable entanglement has a direct physical interpretation. Unfortunately, it is extremely difficult to compute unless the initial state is pure, in which case it reduces to the entropy of entanglement. The entanglement of formation is an upper bound on the distillable entanglement (i.e., one cannot extract more EPR pairs than the number used to form the state).

There exists another entanglement monotone, the logarithmic negativity, which, like the entanglement of formation, provides an upper bound on the distillable entanglement but is also *computable* for mixed states [27]. The logarithmic negativity is defined as

$$E_{\mathcal{N}}(\rho,\{A,B\}) \equiv \log_2[2\mathcal{N}(\rho,\{A,B\})+1], \tag{10}$$

where $\mathcal{N}(\rho,\{A,B\})$ is the negativity of the state ρ. The negativity is defined as the absolute sum of the negative eigenvalues of the partial transpose with respect to A, ρ^{T_A}. So

$$\mathcal{N}(\rho,\{A,B\}) \equiv \sum_i \frac{|\lambda_i|-\lambda_i}{2}, \tag{11}$$

where λ_i are all of the eigenvalues.

The logarithmic negativity can be directly computed from the partial transpose. However, both the logarithmic negativity and the distillable entanglement are zero for those entangled states with positive partial transposes (PPTs). PPT entangled states and perhaps some other entangled states [28,29] have zero distillable entanglement [30]. These states are known as *bound entangled states*.

As with all monotones, the negativity may also disagree with other monotones, such as the entanglement of formation, in which the state of two is more entangled [22]. This ordering problem is a caveat which qualifies many statements about entanglement, and is a reflection of the fact that any given entanglement measure refers only to its own limited physical context.

D. Schmidt decomposition

For a given partition $\{A,B\}$ of the full ensemble's Hilbert space, it is possible to decompose the state as [31]

$$|\Psi\rangle = \sum_{i\in A}\sum_{j\in B} c_{ij}|i\rangle_A|j\rangle_B, \tag{12}$$

where the kets $\{|i\rangle_A,|j\rangle_B\}$ provide complete bases for A and B, respectively. For separable pure states, the matrix $\mathbf{c}$, which is not necessarily square, is rank one, $R(\mathbf{c})=1$. States where $R(\mathbf{c})>1$ are entangled because they cannot be expressed as a single tensor product.

Generally, the Schmidt basis is taken to be diagonal in A. It can be found from the matrix elements c_{ij} by performing a singular-value decomposition of $\mathbf{c}$,

$$\mathbf{c} = \mathbf{U}\Lambda\mathbf{V}^\dagger, \tag{13}$$

where Λ is diagonal and the rows of $\mathbf{U}$ provide the Schmidt basis [32]. There are $r=R(\mathbf{c})$ nonzero elements, $\lambda_1,\ldots,\lambda_r$, along the diagonal of Λ.

Several bipartite entanglement monotones can be defined as functions of the Schmidt coefficients [33,34], however we present this formalism only because the Schmidt decomposition provides an efficient procedure for computing the entropy of entanglement. Starting with a pure state, the reduced entropy for the partition $\{A,B\}$ is given by

$$E(|\Psi\rangle,\{A,B\}) = -\sum_{i=1}^{r} \lambda_i^2 \log_2(\lambda_i^2), \tag{14}$$

where λ_i are the singular values from Eq. (13).

III. SYMMETRIC STATES

The preceding section provided motivation for computing partial traces, partial transposes, and Schmidt decompositions. However, for arbitrary N-particle spin-1/2 ensembles, these operations are exponentially difficult to compute because a general state of the ensemble resides in the space $\mathbb{C}_2^{\otimes N}$ and the dimensions of the density matrix scale as $2^N \times 2^N$. Computational investigation of arbitrary ensemble entanglement is therefore impractical for all but the smallest values of N.

Fortunately, a large number of experimentally relevant states possess symmetry under particle exchange and this property allows us to significantly reduce the computational complexity. A large class of N-particle states are invariant to symmetry transformations of the permutation group

$$\Pi_{ij}\rho_N\Pi_{ij}^\dagger = \rho_N, \quad \forall\, \Pi_{ij}, \tag{15}$$

where the Π_{ij} are operators that exchange particles i and j within the ensemble. This is the most general class of states that are exchange invariant; however, it is also possible to further restrict the space of accessible states to those that are symmetric with respect to single-sided permutations

$$\Pi_{ij}\rho_N = \rho_N, \quad \forall\, \Pi_{ij} \tag{16}$$

of the individual spins. This symmetry further constrains the diagonal terms of the density matrix. For the example of a two-spin system, single-sided symmetry requires $\langle 01|\rho|01\rangle = \langle 10|\rho|01\rangle$, while the more general double-sided symmetry does not.

The states $|m,N\rangle$ that respect this single-sided permutation symmetry compose the symmetric subspace $\mathbb{S}_N$. The ket

$|m,N\rangle$ is defined as the unnormalized N-particle symmetric state with m excitations (spins up),

$$|m,N\rangle \equiv \sum_i P_i(|1_1,1_2,\ldots,1_m,0_{m+1},\ldots,0_N\rangle), \quad (17)$$

where $\{P_i\}$ is the set of all $\binom{N}{m}$ distinct permutations of the spins. Although each $|m,N\rangle$ is an element of $\mathbb{C}_2^{\otimes N}$, the permutation symmetry enables it to be expressed as an element $|\tilde{m}\rangle$ of a space $\mathbb{S}_N$ that scales linearly, rather than exponentially, with the number of particles. In short, all states in $\mathbb{S}_N$ can be represented in $\mathbb{C}_{N+1}$.

The symmetric subspace therefore provides a convenient, albeit idealized, computationally accessible class of spin states relevant to many experimental situations (such as spin squeezing). Completely symmetric systems are experimentally interesting, largely because it is often easier to nonselectively address an entire ensemble of particles rather than individually address each member. Of course, there are still technical challenges in preserving *perfect* symmetry among the particles in an ensemble, such as maintaining the uniformity of magnetic and optical fields. Still, for a system of many particles, symmetrically manipulating the ensemble generally requires fewer resources than addressing individual members.

It is therefore interesting to consider computing various measures of entanglement and simulating the system's dynamics using symmetric states. However, analyzing entanglement requires at least the operations of partial traces and partial transposes. In order for these operations to be practical for large N, it is essential to compute them in an efficient manner, i.e., without having to work with representations of states in the full space $\mathbb{C}_2^{\otimes N}$.

In this section, we derive relationships that allow us to work with arbitrary bipartite splits of the symmetric subspace. The ability to express a symmetric state in terms of tensor products of smaller symmetric states is a critical prerequisite for efficiently computing bipartite entanglement measures. In Sec. III A, we derive the necessary expressions for expressing symmetric states in reduced dimensional bases. These results lead to the operations of partial traces, partial transposes, and Schmidt decompositions on symmetric states. In all of these cases, it is possible to manipulate symmetric states with a worst polynomial scaling of the required computational resources.

A. Symmetric change of basis and decomposition operators

When working with the symmetric subspace, it is necessary to convert between the large $\mathbb{C}_2^{\otimes N}$ and small $\mathbb{C}_{N+1}$ basis representations of the state. In order to provide a systematic means for changing bases, it is convenient to define a symmetry operator, $S_N:\mathbb{C}_2^{\otimes N}\rightarrow\mathbb{C}_{N+1}$, whose action on the density operator in the 2^N-dimensional basis,

$$\tilde{\rho}_N = S_N \rho_N S_N^\dagger \quad (18)$$

projects the state into $\mathbb{S}_N$ expressed in an $(N+1)$-dimensional basis. We have adopted the notation that $\tilde{\rho}_N$ is the symmetric density matrix represented in $\mathbb{C}_{N+1}$.

S_N is an $[(N+1)\times 2^N]$-dimensional matrix that can be expressed as

$$S_N = \sum_{m=0}^{N} C_{N,m} |\tilde{m}\rangle\langle m,N|, \quad (19)$$

where the coefficients are given by

$$C_{N,m} = \binom{N}{m}^{-1/2} = \left[\frac{N!}{m!(N-m)!}\right]^{-1/2} \quad (20)$$

and $C_{N,m}|m,N\rangle$ is the normalized version of Eq. (17). The state $|\tilde{m}\rangle$ is physically the same as the 2^N-dimensional state $|m,N\rangle$ (both have m spins up), except that $|\tilde{m}\rangle$ is normalized and expressed in the $(N+1)$-dimensional basis;

$$\langle\tilde{m}|\tilde{n}\rangle = \delta_{m,n}, \quad (21)$$

$$S_N C_{N,m}|m,N\rangle = |\tilde{m}\rangle. \quad (22)$$

It should be noted that S_N is not a permutation operator, but rather a projector. Therefore, it is only appropriate to operate on symmetric states with S_N as

$$S_N S_N^\dagger = \mathbb{1}_{\text{sym}}, \quad (23)$$

$$S_N^\dagger S_N \neq \mathbb{1}_{\text{full}}, \quad (24)$$

where $\mathbb{1}_{\text{sym}}$ is the identity in the $(N+1)$-dimensional symmetric basis and $\mathbb{1}_{\text{full}}$ is the identity in the 2^N-dimensional full basis. Consequently, $S_N^\dagger S_N \rho_N S_N^\dagger S_N = \rho_N$, only if ρ_N is symmetric. Acting on a nonsymmetric state with S_N and $S_N^\dagger$ results in a loss of information, as the nonsymmetric components of that state are lost in the projection onto $\mathbb{S}_N$.

For the purpose of making a bipartite split $\{A,B\}$, the essential property of the symmetric subspace is that it can be expressed as a tensor product of smaller symmetric spaces. However, the tensor product of arbitrary symmetric states is not necessarily symmetric,

$$\mathbb{S}_N \subset \mathbb{S}_{N-k}\otimes\mathbb{S}_k, \quad (25)$$

where the partition $\{A,B\}$ has been denoted by the number of spins in each subsystem, $\{N-k,k\}$. $\mathbb{S}_{N-k}\otimes\mathbb{S}_k$ is larger than $\mathbb{S}_N$. The structure of valid symmetric products is given by the relation [19]

$$|m,N\rangle = \sum_{p=0}^{k} |m-p,N-k\rangle\otimes|p,k\rangle \quad (26)$$

in terms of constituent symmetric states expressed in the large basis.

Equations (25) and (26) raise the point that the N-particle symmetric space $\mathbb{S}_N$ is smaller than the product space, $\mathbb{S}_{N-k}\otimes\mathbb{S}_k$. Therefore, the entanglement of states in $\mathbb{S}_N$ will generally be more restricted than those in the tensor product space.

While, it is straightforward to identify the maximal entanglement bounds for states in $\mathbb{S}_{N-k}\otimes\mathbb{S}_k$, the same is not true for $\mathbb{S}_N$. Therefore, it is convenient to use the product space entanglement bounds as an upper limit, *albeit an overestimate*, for the scaling of states in $\mathbb{S}_N$.

In order to exploit the tensor product structure in Eq. (26), motivated by our desire to consider bipartite entanglement measures, it is beneficial to construct a new symmetry operator $T_{N-k,k}$, that maps symmetric states into the tensor product structure imposed by the partition $\{N-k,k\}$. In order to be useful for computations, both $\mathbb{S}_{N-k}$ and $\mathbb{S}_k$ must be expressed in their respective small bases. That is, we require the mapping $T_{N-k,k}:\mathbb{C}_{N+1}\rightarrow\mathbb{C}_{N-k+1}\otimes\mathbb{C}_{k+1}$.

Constructon of the operator $T_{N-k,k}$ can be accomplished by decomposing S_N according to Eq. (26),

$$S_N=\sum_{q=0}^{N} C_{N,q}|\tilde{q}\rangle\left[\sum_{p=0}^{k}\langle q-p,N-k|\otimes\langle p,k|\right] \tag{27}$$

and then operating on the expanded $S_N^\dagger$ with both S_{N-k} and S_k,

$$T_{N-k,k}=\sum_{q=0}^{N}\sum_{p=0}^{\min(q,k)}\frac{C_{N,q}}{C_{N-k,q-p}C_{k,p}}|\widetilde{q-p}\rangle_{N-k}\otimes|\tilde{p}\rangle_k\langle\tilde{q}| \tag{28}$$

to produce the necessary mapping. Here, $|\tilde{m}\rangle_{N-k}\in\mathbb{C}_{N-k+1}$ denotes symmetric states in the subsystem A and the $|\tilde{n}\rangle_k\in\mathbb{C}_{k+1}$ are symmetric states in B. Equation (28) has the interpretation of taking an $|\tilde{m}\rangle\in\mathbb{S}_N$, changing back to the large basis, extracting the tensor product structure, and then reducing the dimensions of the subsystems down to their respective small bases.

B. Partial traces in the symmetric subspace

In this section, we derive an expression for

$$\tilde{\rho}_{N-k}=\mathrm{Tr}_k[\tilde{\rho}_N] \tag{29}$$

that avoids expressing any of the density matrices (in any intermediate step) in their large bases. The structure of the operator $T_{N-k,k}$ immediately indicates that this is possible since symmetric states can be expressed as tensor products of lower-dimensional symmetric states. Once the symmetric system has been partitioned, the partial trace is immediate.

Although the operator $T_{N-k,k}$ can be directly applied to $\tilde{\rho}_N$, this approach condenses several intermediate steps that might be useful when performing calculations. Instead, we first convert $\tilde{\rho}_N$ back to the large basis

$$\rho_N=S_N^\dagger\tilde{\rho}_N S_N, \tag{30}$$

$$\rho_N=\sum_{m,n=0}^{N}\frac{\langle m,N|\rho_N|n,N\rangle|m,N\rangle\langle n,N|}{C_{N,m}^{-2}C_{N,n}^{-2}}, \tag{31}$$

and then partition the symmetric states, $|m,N\rangle$ and $|n,N\rangle$, using Eq. (26) with $k=1$. Taking the partial trace of the resulting expression leads to an $(N-1)$-particle symmetric state in the large basis

$$\mathrm{Tr}_1[\rho_N]=\sum_{m,n=1}^{N}C_{N,m}C_{N,n}\langle m,N|\rho_N|n,N\rangle[|m,N-1\rangle\times\langle n,N-1|+|m-1,N-1\rangle\langle n-1,N-1|], \tag{32}$$

which can be changed to the small basis using the operators S_{N-1} and $S_{N-1}^\dagger$,

$$\langle\tilde{a}|\tilde{\rho}_{N-1}|\tilde{b}\rangle=C_{N-1,a}^{-1}C_{N-1,b}^{-1}[\langle\tilde{a}|\tilde{\rho}_N|\tilde{b}\rangle C_{N,a}C_{N,b}+\langle\widetilde{a+1}|\tilde{\rho}_N|\widetilde{b+1}\rangle C_{N,a+1}C_{N,b+1}. \tag{33}$$

By induction, it can be shown that the result of tracing k particles out of the system is

$$\langle\tilde{a}|\tilde{\rho}_{N-k}|\tilde{b}\rangle=\sum_{j=0}^{k}\langle\widetilde{a+j}|\tilde{\rho}_N|\widetilde{b+j}\rangle C_{k,j}^{-2}\frac{C_{N,a+j}C_{N,b+j}}{C_{N-k,a}C_{N-k,b}}, \tag{34}$$

which resides within $\mathbb{C}_{N-k+1}$.

C. Partial transposes in the symmetric subspace

The structure of $T_{N-k,k}$ demonstrates that the partial transpose of symmetric states with respect to k particles, $\tilde{\rho}_N^{T_k}$, resides in the space $\mathbb{S}_{N-k}\otimes\mathbb{S}_k^T$, but not $\mathbb{S}_N$. Therefore, the partial transpose involves matrices that belong to $\mathbb{C}_{k+1}\otimes\mathbb{C}_{N-k+1}$, and computing $\tilde{\rho}_N^{T_k}$ scales quadratically in N.

As with the partial trace, the operator $T_{N-k,k}$ can be directly employed to obtain the partial transpose; however, this approach hides several useful intermediate steps. Instead, a more explicit derivation involves transforming $\tilde{\rho}_N$ back to the big basis and employing Eq. (26). The partial transpose

$$\rho_N^{T_k}=\sum_{m,n=0}^{N}\sum_{p,q=0}^{k}C_{N,m}C_{N,n}\langle\tilde{m}|\tilde{\rho}_N|\tilde{n}\rangle\times[|m-p,N-k\rangle\langle n-q,N-k|\otimes|q,k\rangle\langle p,k|] \tag{35}$$

can be expressed as a tensor product

$$\rho_N^{T_k}\equiv\sum_{p,q=0}^{k}A_{N-k}^{p,q}\otimes B_k^{p,q}, \tag{36}$$

where

$$A_{N-k}^{p,q}=\sum_{m,n=0}^{N}C_{N,m}C_{N,n}\langle\tilde{m}|\tilde{\rho}_N|\tilde{n}\rangle|m-p,N-k\rangle\langle n-q,N-k| \tag{37}$$

and

$$B_k^{p,q}=|q,k\rangle\langle p,k|. \tag{38}$$

Return to the small basis is accomplished by evaluating, $\tilde{A}^{p,q}_{N-k}=S_{N-k}A^{p,q}_{N-k}S^{\dagger}_{N-k}$ and $\tilde{B}^{p,q}_{k}=S_k B^{p,q}_k S^{\dagger}_k$ to give

$$\langle\tilde{a}|\tilde{A}^{p,q}_{N-k}|\tilde{b}\rangle=\frac{C_{N,p+a}C_{N,q+b}}{C_{N-k,a}C_{N-k,b}}\langle\widetilde{a+p}|\tilde{\rho}_N|\widetilde{b+q}\rangle, \quad (39)$$

$$\langle\tilde{c}|\tilde{B}^{p,q}_{k}|\tilde{d}\rangle=C^{-1}_{k,c}C^{-1}_{k,d}\delta_{q,c}\delta_{p,d}, \quad (40)$$

where

$$\tilde{\rho}^{T_k}_N=\sum_{p,q=0}^{k}\tilde{A}^{p,q}_{N-k}\otimes\tilde{B}^{p,q}_k \quad (41)$$

shows that the dimension of $\tilde{\rho}^{T_k}_N$ is, in fact, $(k+1)\times(N-k+1)$.

D. Schmidt decomposition of the symmetric subspace

It is quite simple to perform the Schmidt decomposition, Eq. (12), of a symmetric state in $\mathbb{S}_N$, into the space $\mathbb{S}_{N-k}\otimes\mathbb{S}_k$. The coefficients c in Eq. (12) for the states $|\tilde{m}\rangle$ follow directly from applying the operator $T_{N-k,k}$ to $|\tilde{m}\rangle$, resulting in the expression

$$T_{N-k,k}|\tilde{m}\rangle=\sum_{i=0}^{N-k}\sum_{j=0}^{k}\delta_{m,i+j}\frac{C_{N,m}}{C_{N-k,i}C_{k,j}}|\tilde{i}\rangle_{N-k}\otimes|\tilde{j}\rangle_k. \quad (42)$$

For the states $|\tilde{m}\rangle$ the Schmidt matrix c is sparse and the singular-value decomposition, Eq. (13), can be performed analytically.

General symmetric states, $|\tilde{\Psi}\rangle=\Sigma_{m=0}^{N}a_m|\tilde{m}\rangle$, can be represented as

$$T_{N-k,k}|\tilde{\Psi}\rangle=\sum_{m=0}^{N}a_m\sum_{i=0}^{N-k}\sum_{j=0}^{k}\delta_{m,i+j}\frac{C_{N,m}}{C_{N-k,i}C_{k,j}}|\tilde{i}\rangle_{N-k}|\tilde{j}\rangle_k. \quad (43)$$

However, for these general symmetric states, the Schmidt coefficient matrix c is not sparse.

E. Dynamics in the symmetric space

One of the objectives of this paper is to treat dynamically generated entangled states, therefore, this section briefly discusses the time evolution of symmetric states. It is straightforward to show that acting on a symmetric state with operators of the form

$$\mathbf{o}=\sum_{j=1}^{N}\mathbb{1}^{(1)}\otimes\cdots\mathbf{o}^{(j)}\cdots\otimes\mathbb{1}^{(N)} \quad (44)$$

preserves the exchange symmetry in the large basis, $[\mathbf{o},\Pi_{ij}]=0$, provided that the $\mathbf{o}^{(i)}$ are identical.

Using the symmetric state change of the basis operator S_N elucidates the physical nature of the symmetric subspace. For example, transforming any angular-momentum operator of the form in Eq. (44) to the small basis using S_N,

$$\tilde{\mathbf{J}}=S_N\mathbf{J}S^{\dagger}_N=S_N\left(\sum_i\mathbf{j}^{(i)}\right)S^{\dagger}_N \quad (45)$$

produces the $(N+1)$-dimensional operator equivalent to the angular momentum for a single *pseudospin* $(J=N/2)$ particle. This is because the symmetric subspace is composed of basis states $|\tilde{m}\rangle$ that correspond to the eigenstates of J_z with $J=N/2$ (e.g., for two spins, the symmetric subspace includes the triplet, but not the singlet).

The dynamics of any symmetric state are confined to the symmetric subspace, provided that the Hamiltonian can be expressed as a function of operators all of the form as in Eq. (44). Given a symmetry-preserving Hamiltonian, the dynamics can be completely simulated with the small symmetric basis. Explicitly, an infinitesimal step of evolution can be written

$$\begin{aligned}|\tilde{\Psi}(t+dt)\rangle&=S_N(1+iHdt)|\Psi(t)\rangle\\&=S_N|\Psi(t)\rangle+idtS_NH|\Psi(t)\rangle\\&=S_N|\Psi(t)\rangle+idtS_NHS^{\dagger}_NS_N|\Psi(t)\rangle\\&=|\tilde{\Psi}(t)\rangle+idt\tilde{H}|\tilde{\Psi}(t)\rangle,\end{aligned} \quad (46)$$

where we have used $|\tilde{\Psi}(t)\rangle=S_N|\Psi(t)\rangle$, $\tilde{H}\equiv S_NHS^{\dagger}_N$, and $|\Psi(t)\rangle=S^{\dagger}_NS_N|\Psi(t)\rangle$ [because $|\Psi(t)\rangle$ is assumed to be symmetric].

For many experimentally motivated N-particle spin-1/2 systems, it is possible to express states using the symmetric subspace and the dynamics using only symmetry-preserving operators. The only time this efficient representation fails to apply is when the symmetry is broken or the system is divided (as we consider throughout the paper). For example, the spontaneous local decay of any one spin is sufficient to break the symmetry of Eq. (16). Depending on the form of the decoherence, some symmetry may be retained [e.g., the particle exchange symmetry of Eq. (15)]. Other treatments have addressed the effect of such decoherence on parameters related to entanglement, such as the degree of spin squeezing [9,15,16].

IV. ENTANGLEMENT PROPERTIES FOR REPRESENTATIVE SYMMETRIC STATES

Given the large number of possible N-spin states, even when restricted to the symmetric space, it is clear that a systematic, yet compact approach to characterize microscopic entanglement is necessary. Toward this end, we characterize a set of representative symmetric states with a limited combination of measures, including the reduced state entropy, the entanglement of formation, and the logarithmic negativity. The families (described in detail below) that we have selected display diverse entanglement behavior—they differ in their degree of entanglement at different size scales and in their robustness to particle loss. Naturally, any set of representative states will be incomplete in some aspect; however, our goal is to provide a detailed picture of internal

entanglement without an excessive number of representatives.

In this section, we address the relationship between the degree of entanglement and its robustness to particle loss. While it has been a longstanding conception that the most entangled states are simultaneously the most fragile, we demonstrate that this is not necessarily true. Under certain useful definitions of entanglement, it is possible to find heavily entangled symmetric states that are simultaneously robust. Similarly, the most fragile states are not always the most entangled. We also demonstrate that restricting our analysis to the symmetric subspace does not preclude the potential for significant entanglement.

A. Symmetric reference states

We now briefly describe several families of representative symmetric states using the notation introduced in Sec. III. In addition to GHZ states and the *W* family, we introduce a parametrized family, termed ''comb states,'' which prove important in investigating the maximal boundary of certain entanglement measures.

In the rest of this paper, all states are assumed to be symmetric. In the interest of simpler notation, we will express symmetric states as ρ even when it is more efficient to compute entanglement measures using their $\tilde{\rho}$ representation. Tilde notation is used only for the $|\tilde{m}\rangle$ states.

1. GHZ states

The well-known GHZ states [35] can be written

$$|\mathrm{GHZ}\rangle = (|\tilde{0}\rangle + |\tilde{N}\rangle)/\sqrt{2} \tag{47}$$

using the notation from Sec. III. The GHZ family is generally considered to be the standard example of a highly entangled state. In several different contexts, it has become the common unit of entanglement currency. For example, as a particular Bell state, the GHZ state is the desired product of entanglement distillation protocols.

However, the GHZ family fails to maximize a number of monotones, including the entanglements of distillation and formation for a given bipartite split. Unlike previous treatments [19], we choose to work with these measures under which the GHZ is not a maximally entangled state. Certain other measures such as the *N tangle* correctly recognize the GHZ as containing the most true *N*-way entanglement [17,34,36], but our focus will remain on notions of strictly bipartite entanglement. Still, the most practical defining characteristic of the GHZ state is its fragility to particle loss; tracing out a single party destroys *all* of the internal entanglement.

2. Dicke states

An important family of states with completely different character is the set of symmetric states with integer *m* excitations (spins up), $|\tilde{m}\rangle$, where $m=0,\ldots,N$. Of course, these states are also known as the Dicke states or the eigenstates of J_z, where the notation $|J,M\rangle$ is used with $J=N/2$ and $M=m-N/2=-N/2,\ldots,N/2$. The *W* state [37], which is defined as the symmetric state with one excitation, $|W\rangle \equiv |\tilde{1}\rangle$, is a particular member of this family. Notice that $|\tilde{m}\rangle$ and $|\widetilde{N-m}\rangle$ have the same entanglement properties because one is equal to the other if the quantization axis is reversed. These states exhibit a high degree of entanglement for $m=1,\ldots,N-1$, while the states of $m=0,N$ are completely separable. The defining characteristic of the Dicke state entanglement is its remarkable robustness to particle loss. It has been proven that $|\tilde{1}\rangle$ optimizes the concurrence when all but two spins have been removed [38], the extreme opposite of the fragile GHZ behavior. It has also been proven that for single copies, the GHZ and *W* cannot be converted into each other with LOCC operations on the individual spins with certainty [37], further emphasizing their difference. For additional discussions of the conversion properties of entangled states, see [39–41].

3. Comb states

A parametrized family of practical importance which we call comb states is defined as

$$|\mathrm{C}(s)\rangle = \sqrt{\frac{2s}{N}} \sum_{m=-N/s}^{N/s} |\widetilde{N/2+ms}\rangle. \tag{48}$$

In the $|\tilde{m}\rangle$ basis, these states have a comblike structure with *m*-independent weighting for the nonzero elements which are spaced by *s* excitations. Since the comb states nontrivially explore the full support of the symmetric basis, they may be expected to access regions of entanglement space where $|\tilde{m}\rangle$ states are forbidden. We find that particular comb states with an optimized spacing *s* turn out to contain near-maximal entanglement for bipartite splits of any symmetric ensemble as will be shown numerically and proven in the Appendix.

4. Random states

Another way to numerically explore the full symmetric space is randomly. We define a randomly generated state $|R\rangle = \Sigma_m r_m |\tilde{m}\rangle$, where the coefficients r_m are complex Gaussian random variables with averages $E[r_m]=0$, $E[r_m r_n]=0$, and $E[r_m^* r_n]=\delta_{mn}/(N+1)$. Note that this distribution of states is independent of the basis, in terms of which we have chosen to define the random coefficients r_m. If we write $|R\rangle = \Sigma_m r'_m (U|\tilde{m}\rangle)$ in a new basis $U|\tilde{m}\rangle$, where U is an arbitrary unitary transformation, the new coefficients r'_m have exactly the same Gaussian distribution as the coefficients r_m. As a result, this distribution determines a measure of (unnormalized) vectors in $\mathbb{C}_{N+1}$ that is invariant under unitary transformations. Moreover $E[\langle \mathrm{R}|\mathrm{R}\rangle]=1$ so the states are on an average normalized and, in fact, the distribution of norms becomes very sharply peaked around 1 as $N\to\infty$. In this limit, we can regard the states $|R\rangle$ as being drawn from the natural unbiased distribution of pure states. In practice, we randomly select these vectors for a fixed finite *N* of interest and normalize.

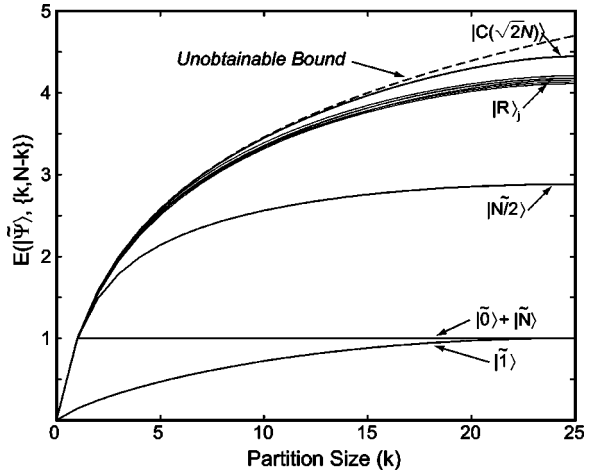

FIG. 1. Entropy of entanglement for representative symmetric states (described in Sec. IV) with $N=50$ particles as a function of the dimension of the bipartite split, $\{k,N-k\}$, where $k=1,\ldots,\lfloor N/2\rfloor$. The *unobtainable bound* $\log_2(k+1)$ is the entropy that could be achieved by a nonsymmetric product of the two symmetric subsystems $\{A,B\}$. Several representative states nearly achieve this maximum.

B. Pure state entropy of entanglement

For an initially pure, N-particle symmetric state, there are $\lfloor N/2\rfloor$ possible ways to partition the system into two parts. With symmetric states we can replace the labeling of a particular partition $\{A,B\}$ with the number of spins in each partition $\{N_A=k,N_B=N-k\}$, where $k=1,\ldots,\lfloor N/2\rfloor$. The entropy can then be computed from either of the reduced density matrices [23], $\rho_{N-k}=\mathrm{Tr}_k\rho_N$ or $\rho_k=\mathrm{Tr}_{N-k}\rho_N$:

$$E(|\Psi\rangle,\{k,N-k\})=S(\mathrm{Tr}_k|\Psi\rangle\langle\Psi|)=S(\mathrm{Tr}_{N-k}|\Psi\rangle\langle\Psi|). \tag{49}$$

It can be proved that the entropy is a monotonically increasing, concave down-function of k in this range [42]. (From this point on, we implicitly assume the rounding of noninteger numbers such that $\lfloor N/2\rfloor$ is implied by $N/2$ and $\{\lfloor N/2\rfloor,\lceil N/2\rceil\}$ is implied by $\{N/2,N/2\}$.)

In Sec. III A, we emphasized that a symmetric state with N particles can be represented on the product space of two symmetric spaces with $N-k$ and k particles ($\mathbb{S}_{N-k}\otimes\mathbb{S}_k$). For all states within this space, the state of Eq. (5) (with $d_A=k+1$) maximizes $E(|\Psi\rangle,\{k,N-k\})$ at $\log_2(k+1)$. However, this state is *not* symmetric with respect to the exchange of any two particles across the split. We are interested in finding the upper bound for the states in the space $\mathbb{S}_N$, which are only a subset of states in $\mathbb{S}_{N-k}\otimes\mathbb{S}_k$. It has been proven that the additional restriction of overall symmetry constrains the maximal entropy to be strictly less than $\log_2(k+1)$, except for $N=2,3,4$, and 6 where states that achieve this bound can be found [19]. Consequently, we refer to the bound $\log_2(k+1)$ as the *unobtainable bound* for any k.

Figure 1 shows a plot of $E(|\Psi\rangle,\{k,N-k\})$ for several reference states and $N=50$. Despite the fact that all states are forbidden from achieving the value $\log_2(k+1)$, some states come close to achieving this unobtainable bound. These include most randomly generated states and the comb states with $s=\sqrt{2N}$. This naturally leads us to the question: what exactly is the minimum upper bound for the split entropy of symmetric states and what states achieve this bound?

1. Maximizing the even split entropy

Since the entropy is maximized by the most even split ($k=N/2$), we henceforth consider only this partition. From the above discussion, we know that for $N\geqslant 7$, the entropy obeys the inequalities

$$E(|\Psi\rangle,\{N/2,N/2\})\leqslant E_{max}(N)<\log_2(N/2+1). \tag{50}$$

Analytically, locating the minimum upper bound $E_{max}(N)$ (or the states that achieve it) is difficult, but a simple numeric approach turns out to shed some light on what we can ex-

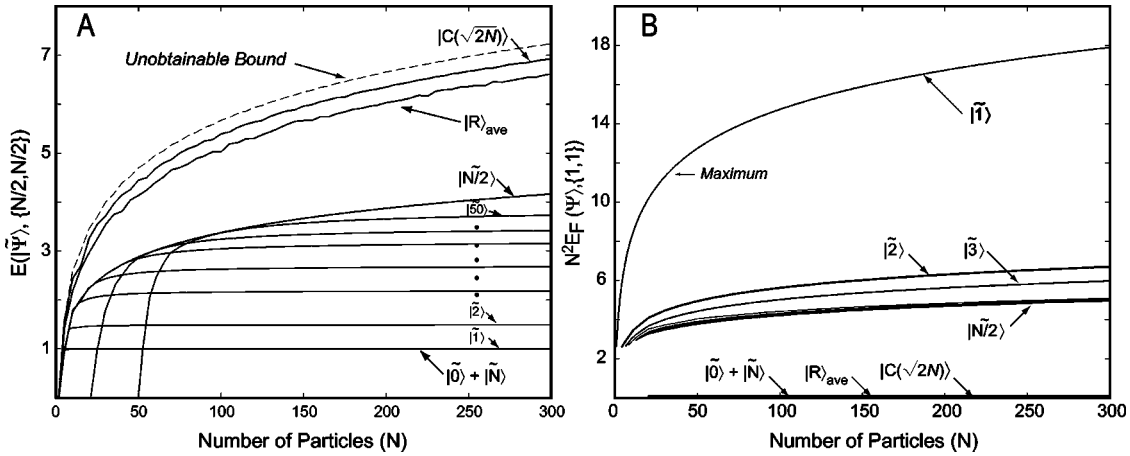

FIG. 2. (a) Plot of the even split entropy of entanglement, $E(\rho,\{N/2,N/2\})$, for representative states as a function of the number of particles, N (which is also equal to the entanglement of formation and distillation). Note that the average entropy of 25 random states, $|R\rangle$, as well as the entropy of $|C(\sqrt{2N})\rangle$, nearly attain the *unobtainable bound* $\log_2(\lfloor N/2\rfloor+1)$. (b) A plot of the two-particle entanglement of formation, $E_F(\rho,\{1,1\})$, as a function of the number of particles, N. The W state $|\tilde{1}\rangle$ maximizes this entanglement measure, which quantifies robustness to particle loss.

pect. Figure 2(a) shows the entropy of the even split entropy as a function of N for several families of states with the unobtainable upper bound for reference. Most families of states do not keep up with the scaling of this upper bound.

For example, if $N \gg m$, the states $|\widetilde{m}\rangle$ (with $m = 1, \ldots, N/2$) can be shown to have entropies of

$$E(|\widetilde{m}\rangle, \{N/2, N/2\}) \approx \frac{\log_2(m)}{2} + 1. \tag{51}$$

We also see that the largest of these scales as $E(|\widetilde{N/2}\rangle, \{N/2, N/2\}) \approx \log_2(N)/2$.

Due to the factor of 2, none of these states keep up with the $\mathrm{S}_{N/2} \otimes \mathrm{S}_{N/2}$ bound. However, if we explore the simplest possible states accessing more of the symmetric Hilbert space, we find something quite different. For large N (up to 600), the average entropies of random states, for example, numerically scale as $\approx \log_2(N/2+1) - 0.6$. This indicates the remarkable fact that the symmetry constraint on the overall state does not limit the *scaling* of the maximal bipartite entanglement compared to that of the more general space $\mathrm{S}_{N/2} \otimes \mathrm{S}_{N/2}$.

The comb states, optimized over the spacing s, are even more entangled. Numerically, we find that (for N up to 600) their entropies scale as $\approx \log_2(N/2+1) - 0.3$, when $s \approx \sqrt{2N}$. Encouraged by this evidence, we were able to prove in the asymptotic limit of large N that this family of comb states $|C(\sqrt{2N})\rangle$ does indeed scale as $\log_2(N/2+1) - \delta$, where δ is a constant of order unity (see the Appendix). A similar proof for the random state scaling is probably possible. The fact that random states, and the optimized comb state, seem to nearly maximize the $\{N/2, N/2\}$ entropy indicates that the set of states which scale similarly is of nonzero measure (i.e., this behavior is not atypical).

Still we have not located the value of the true minimum upper bound and the form of the states that achieve this bound. Given the above results, we expect it to have a similar scaling with a minimal offset δ for large N.

C. Entanglement of formation: Extremal splits

For any bipartite entanglement measure, we can construct even more possible splits if we choose (or are forced) to ignore some of the particles. Suppose we start with a symmetric state of N spins $|\Psi\rangle$ and trace out spins until only N_r remain. In this case, the new state $\rho_{N_r} = \mathrm{Tr}_{N-N_r}(|\Psi\rangle\langle\Psi|)$ will be mixed but *still* symmetric. We then have the possible bipartite splits $\{k, N_r - k\}$ with $k = 0, \ldots, N_r/2$ [53].

For pure states, the entropy of entanglement for any bipartite split is equal to both the entanglement of formation and distillation. Unfortunately, numerically calculating either of these monotones is much more difficult if given an initially mixed density matrix. For negativities, we showed in Sec. III C that we can numerically calculate all bipartite splits $\{k, N_r - k\}$ for symmetric states, and we will demonstrate this ability in Sec. IV D. For now, we would like to deal with the extreme case of all but two spins removed ($N_r = 2$). In Sec. II B, we stated that the entropy of formation $E_F(|\Psi\rangle, \{1,1\})$ is easily calculated for two spin mixed states through the concurrence. By discussing the relationship of the pair $[E_F(|\Psi\rangle, \{1,1\}), E_F(|\Psi\rangle, \{N/2, N/2\})]$, we can start to get the meaning of the allowed relationship of entanglement across the extremes of size scales. We will refer to the splits $\{1,1\}$ and $\{N/2, N/2\}$ as the *extremal splits*.

Figure 2(b) displays $E_F(|\Psi\rangle, \{1,1\})$ for several reference states. It has been proven that the W state $|\widetilde{1}\rangle$ maximizes the concurrence, hence also the entanglement of formation (for all symmetric states) with a value of $\mathcal{C}(|\widetilde{1}\rangle) = 2/N$ [13,38]. Wang and Mølmer [10] have shown that by using a similar formalism, where the two-spin concurrences are calculated from the moments of the entire state, analytic expressions can be derived for the concurrences of several families of symmetric states. In particular, for the Dicke states $|\widetilde{m}\rangle$, and $M = m - N/2$, the concurrence is

$$\mathcal{C}(|\widetilde{M+N/2}\rangle) = \frac{1}{2N(N-1)}\{N^2 - 4M^2 - \sqrt{(N^2-4M^2)[(N-2)^2-4M^2]}\}, \tag{52}$$

which gives the above result for the $|\widetilde{1}\rangle$ state and also $\mathcal{C}(|\widetilde{N/2}\rangle) = 1/(N-1)$. In the large-$N$ limit, these concurrences lead to the entanglements of formation

$$E_F(|\widetilde{1}\rangle, \{1,1\}) \approx \frac{2\log_2 N + \log_2 e}{N^2}, \tag{53}$$

$$E_F(|\widetilde{N/2}\rangle, \{1,1\}) \approx \frac{2\log_2 2(N-1) + \log_2 e}{[2(N-1)]^2}. \tag{54}$$

The $1/N^2$ scaling is due to the fact that the two-spin state is constrained to be reduced from a larger symmetric-N spin state. In effect, one spin can only be so entangled with another when it is constrained to have the same relationship with all other spins.

For many states $E_F(|\Psi\rangle, \{1,1\})$ is simply zero. The GHZ state, the comb state, and practically all random states have zero $\{1,1\}$ entanglement and do not contain the same degree of robust entanglement as the $|\widetilde{m}\rangle$ states. Furthermore, the ordering of states shown in Figs. 2(a) and 2(b) is reversed (with the exception of the GHZ). This leads to the question: what is the nature of the trade-off between the small- and large-scale entanglement of the extremal splits?

Figure 3 shows each state as a point in the space of $[E_F(|\Psi\rangle, \{1,1\}), E_F(|\Psi\rangle, \{N/2, N/2\})]$ for $N = 50$. The line between $|\widetilde{0}\rangle$ and $|\widetilde{1}\rangle$ represents states which are a linear combination of these two states. The curve extending from the $|\widetilde{N/2}\rangle$ state to the vertical axis and up that axis to the comb state represents linear combinations of those two states. The forbidden regions of this space for symmetric states are unknown but we strongly suspect several properties of the boundaries. We conjecture that there are two regions where no states are allowed to exist. First, in region I, beneath the $|\widetilde{0}\rangle \leftrightarrow |\widetilde{1}\rangle$ line, no states are found, nor likely to exist. The

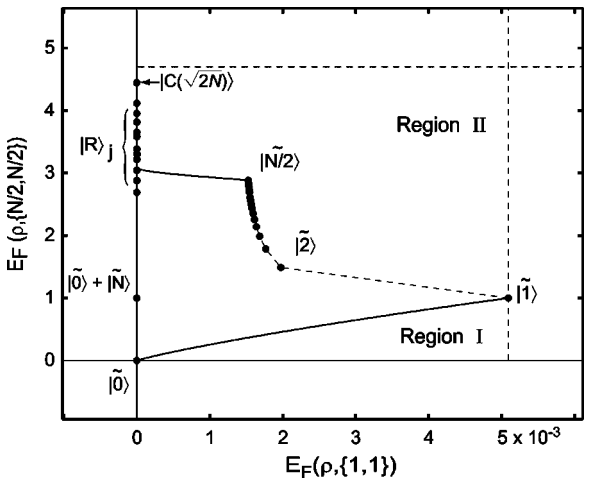

FIG. 3. Plot of accessible entangled states in a space that reflects the trade-off between the degree of entanglement $[E_F(\rho,\{N/2,N/2\})]$ and its robustness to particle loss $[E_F(\rho,\{1,1\})]$. The degree of entanglement for the large split is also equal to the distillable entanglement.

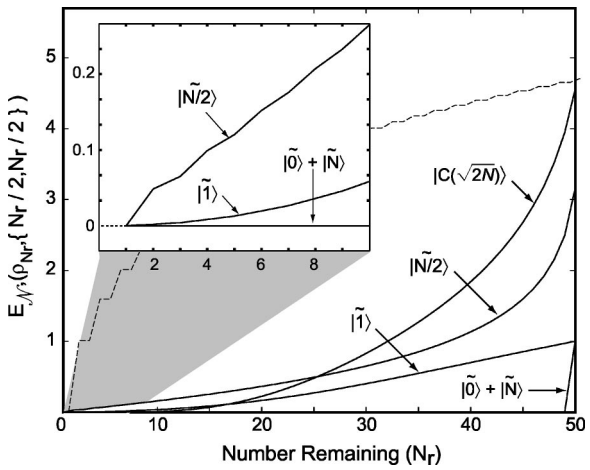

FIG. 4. Plot of the even split negativity, $E_{\mathcal{N}}(\rho,\{N_r/2,N_r/2\})$, for representative symmetric states with $N=50$, as a function of the number of particles remaining, N_r, in the system. The inset plot highlights the particular robustness of the $|\widetilde{N/2}\rangle$ Dicke state as measured by the negativity. This contrasts a similar analysis using the entanglement of formation, where $|\tilde{1}\rangle$ is most robust.

reason for this is that to have any $\{1,1\}$ entanglement, there must exist some degree of $\{N/2,N/2\}$ entanglement. However, there must also be a region in the upper right of region II, where no states exist. It appears that there exists a fundamental trade-off between small- and large-scale entanglement: as the large-scale entanglement of a state increases (and is above 1), the maximum allowable small-scale entanglement, will decrease. In addition, there is likely a critical value of the $\{N/2,N/2\}$ entanglement above which the $\{1,1\}$ entanglement must be zero.

D. Negativities: Extension to all splits

Now that we have a better idea of the relationship between the entanglement of the extremal splits, we can more confidently approach the problem of understanding the large number of remaining splits. For N_r spins remaining, there are $N_r/2$ splits of the form $\{k,N_r-k\}$ with $k=1,\ldots,N_r/2$. If $N_r<N$ and the initial state is nonseparable, the reduced state is mixed and one of the few computable entanglement measures available is the negativity. Even though it is a computable monotone, the negativity is not an entanglement measure with as much physical justification as the entanglement of formation or distillation. However, the logarithmic negativity is an upper bound for the distillable entanglement [27]. With this in mind, we move forward and work with the logarithmic negativities as an indicator of *potential* entanglement.

1. Negativity of all even splits

Before computing the negativities, we can use the properties of monotones to notice a few relationships between the bipartite monotones of different splits. Tracing out a single spin is an operation that falls under LOCC, and any monotone X, including the negativity, can only decrease under such an operation, therefore,

$$E_X(|\Psi\rangle,\{k-1,N_r-k\}) \leqslant E_X(|\Psi\rangle,\{k,N_r-k\}),$$

$$E_X(|\Psi\rangle,\{k,N_r-k-1\}) \leqslant E_X(|\Psi\rangle,\{k,N_r-k\}).$$

For pure states, the most even split $\{N/2,N/2\}$ gives the maximal entropy of entanglement [43]. We observe that this is also true for the most even splits of a reduced mixed state with N_r particles remaining $\{N_r/2,N_r/2\}$. These observations motivate us to reduce the number of splits considered to only the even splits of a given N_r. Figure 4 displays the quantity $E_{\mathcal{N}}(|\Psi\rangle,\{N_r/2,N_r/2\})$ as a function of N_r for several reference states. The end points of this plot give similar information about the extremal splits as the previous description of entanglement of formation. Unlike the entanglement of formation, we can easily plot the intermediate splits for the logarithmic negativity.

By the above inequalities, we know that each curve monotonically increases with N_r. For reference we have included the plot of $\log_2(N_r/2+1)$ which, of course, cannot be achieved, because each reduced state with N_r spins remaining is constrained by the symmetry of the initial pure state. The space between this maximum and the space of all actual curves represents the entanglement ''cost'' of initial symmetrization. An unanswered question is for a given N_r and N: what pure state $|\Psi\rangle$ maximizes $E_{\mathcal{N}}(|\Psi\rangle,\{N_r/2,N_r/2\})$? What is this maximum as a function of N_r and N? These questions for both the negativities and other bipartite monotones are extensions of the problems encountered for the extremal splits. Again, we plot only the reference states and set aside the problem of fully characterizing the space of interest.

First, consider the GHZ state $|\tilde{0}\rangle+|\tilde{N}\rangle$. As expected, this state is maximally fragile, starting at unity and dropping to zero as soon as one spin is removed. In direct contrast, the W state $|\tilde{1}\rangle$ starts at unity, but only slowly decays to zero as spins are removed and its logarithmic negativity remains finite for even $N_r=2$. The state $|\widetilde{N/2}\rangle$ is, in some sense, an

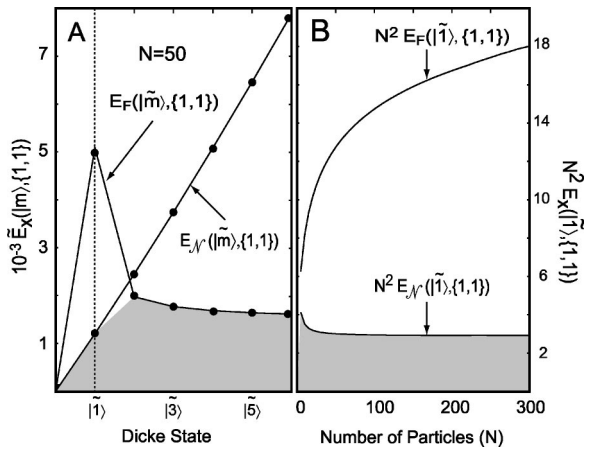

FIG. 5. (a) Plot of the inconsistent ordering of the reduced entanglement of formation, $(E_F(\rho,\{1,1\})$, and the reduced logarithmic negativity, $E_{\mathcal{N}},\{1,1\})$, for Dicke states. The shaded region reflects the possible values for the distillable entanglement. (b) The large-N scaling of the entanglement measures in (a) for the $|\tilde{1}\rangle$ (i.e., W) state.

optimal trade-off between total entanglement and robust entanglement; in that it starts reasonably high above unity at $N_r=N$, but appears to have maximal negativity below $N_r \approx N/2$. The comb states (and random states), which have near-maximal total entanglement, are also a reasonable trade-off, especially compared to the extreme fragility of the GHZ state.

The comb state and most random states still attain zero negativity (no negative eigenvalues of the partial transpose) below a critical N_r. Since the logarithmic negativity is an upper bound on the distillable entanglement, this must also be zero at these points. The size of this critical N_r for a given state is another indicator of fragility of the entanglement (for the GHZ state it is the extreme $N-1$). For the optimal comb state, the size of this critical value appears to scale only logarithmically in N. Thus, the comb states, despite having near-maximal $\{N/2,N/2\}$ entanglement, contain entanglement that can withstand a huge amount of particle loss.

2. Ordering of Dicke states

Given the fact that $|\tilde{1}\rangle$ optimizes the entanglement of formation of the $\{1,1\}$ split, it may seem odd that $|\widetilde{N/2}\rangle$ maximizes the negativity. Indeed, there is an ordering issue here and the two monotones disagree on which of the reduced states is more entangled. See Ref. [22] for a more complete discussion of ordering problems with entropies and entanglement measures for two-spin systems. Figure 5 displays the ordering problem between $E_{\mathcal{N}}(|\tilde{m}\rangle,\{1,1\})$ and $E_F(|\tilde{m}\rangle,\{1,1\})$ for $N=50$. For $N/2 \geqslant j \geqslant 1$, $E_F(|\tilde{j}\rangle,\{1,1\}) > E_F(|\widetilde{j+1}\rangle,\{1,1\})$, whereas $E_{\mathcal{N}}(|\tilde{j}\rangle,\{1,1\}) < E_{\mathcal{N}}(|\widetilde{j+1}\rangle,\{1,1\})$, so the quantities are, respectively, decreasing and increasing with j. In fact, the two curves will always cross because $E_F(|\tilde{1}\rangle,\{1,1\}) > E_{\mathcal{N}}(|\tilde{1}\rangle,\{1,1\})$ and $E_F(|\widetilde{N/2}\rangle,\{1,1\}) < E_{\mathcal{N}}(|\widetilde{N/2}\rangle,\{1,1\})$. For large N, $N^2 E_F(|\widetilde{N/2}\rangle,\{1,1\}) \approx \log_2(N)/2 < N^2 E_{\mathcal{N}}(|\widetilde{N/2}\rangle,\{1,1\}) \approx N\log_2(e)$, where the approximations can be shown both analytically and numerically.

For $N \gg m$, $N^2 E_{\mathcal{N}}(|\tilde{m}\rangle,\{1,1\})$ flattens out to a constant as a function of N, while $N^2 E_F(|\tilde{m}\rangle,\{1,1\})$ continues to grow logarithmically, as shown if Fig. 5(b) for $|\tilde{1}\rangle$. In this case, the entanglement of formation is significantly greater than the logarithmic negativity and hence also the distillable entanglement. So, for the state $|\tilde{1}\rangle$, we can show

$$E_D(|\tilde{1}\rangle,\{1,1\}) \leqslant E_{\mathcal{N}}(|\tilde{1}\rangle,\{1,1\}) \approx \frac{3}{N^2}$$

$$< E_F(|\tilde{1}\rangle,\{1,1\}) \approx \frac{2\log_2 N + \log_2 e}{N^2}. \tag{55}$$

All measures monotonically decrease with N, but the distillable entanglement decreases at least logarithmically faster than the entanglement of formation. Similar statements are possible about any $|\tilde{m}\rangle$, with $N \gg m$.

V. ENTANGLEMENT IN SYMMETRIC DYNAMICALLY GENERATED STATES

Characterizing the reference states enabled us to quantitatively identify the trade-off between the degree of entanglement and robustness to particle loss. This relationship can be expressed as boundaries in the space expressed by the entanglements of formation for the extremal splits. With this relationship in hand, we are now able to address the question of where various dynamically generated states lie with respect to all accessible symmetric states.

For any given generation process, an important question involves exactly how entanglement forms within an ensemble [44]. In this section, we characterize spin-squeezed states, the most common experimental example of large-scale entanglement. It has been shown that spin squeezing [Eq. (1)] is a sufficient condition for an N-particle system to be entangled [11] and the squeezing parameter also indicates in some sense the depth of entanglement [12]. It has also been demonstrated that spin-squeezed systems contain significant pairwise entanglement [9,10]. However, little is known about the entanglement of squeezed states across all size scales or how they compare to the reference states from Sec. IV. Describing such states in terms of entanglement measures is intrinsically important, but also useful for understanding the more general class of symmetric entangled states. At the end of this section, we also briefly discuss the problem of efficiently creating desirable states; given specified resources, allowable processes, and initially separable states.

A. Spin-squeezed states

The collective angular-momentum operators of any multipartite spin state must satisfy the inequalities imposed by their commutation relations. Let us assume, without loss of generality, that all subsequent states satisfy $\langle J_x\rangle = \langle J_y\rangle = 0$

and $\langle J_x^2\rangle = \min_\theta(\langle J_\theta^2\rangle)$, such that x is the direction of the smallest variance perpendicular to the mean which points in the z direction. In this case, we use the uncertainty relationship

$$\langle J_x^2\rangle\langle J_y^2\rangle \geqslant \frac{\langle J_z\rangle^2}{4}. \tag{56}$$

The characteristic feature of spin-squeezed states is that internal correlations between spins (i.e., entanglement) conspire to reduce the noise in one angular-momentum component (x) at the expense of increasing the uncertainty in another (y). In particular, spin-squeezed states satisfy the inequality

$$\xi^2 \equiv \frac{N\langle J_x^2\rangle}{\langle J_z\rangle^2} < 1. \tag{57}$$

States with a minimal squeezing parameter ξ^2 are useful for reducing noise in many interferometric applications (e.g., atomic clocks). Using Eq. (56) and the fact that $\langle J_y^2\rangle < J^2$, one can show that

$$\xi^2 > \frac{1}{N}, \tag{58}$$

where $1/N$ is the Heisenberg limit.

1. Squeezing and entanglement

We choose to generate near-optimally spin-squeezed states $|\Psi_\xi\rangle$ by applying the countertwisting Hamiltonian $H_{ct} = (J_+^2 - J_-^2)/i$ to an initially polarized sample $|\Psi_0\rangle = |\tilde{0}\rangle$ (with $\xi^2 = 1$) for the length of time t_N needed to minimize ξ^2 [2]. This process does not produce optimally squeezed states (see Ref. [12]), but in the large-N limit, it creates states which very nearly obtain the minimal value of ξ^2. The time it takes to reach the minimum of $\xi^2 \propto 1/N$ for large N is $t_N \approx 0.2\log_2(N)/N$ [16]. Henceforth, time is scaled such that the optimal spin-squeezing time $t_N = 1$. We will ignore the small difference between the achieved and optimum spin squeezing, so that we may examine the production of entanglement as the state evolves in the most simple way. Interestingly, an effective countertwisting Hamiltonian can be experimentally realized through the QND detection and feedback rotation scheme of Ref. [8].

Figure 6 shows this evolution for a state with $N = 50$ spins. The x and y means remain zero for the entire evolution, while $\langle J_z\rangle$ decays from completely polarized through zero. For small numbers of spins, the state will quickly recohere and become completely polarized (separable). For large numbers of spins, the dynamics become highly disordered after the mean decays through zero, and the recoherence time grows much longer. After becoming maximally squeezed, the internal entanglement continues to grow, but the spin squeezing rapidly gets worse because of the reduction in the mean. The entanglement of formation for the largest and smallest even splits [$E_F(\rho(t),\{N/2,N/2\})$ and $E_F(\rho(t),\{1,1\})$] are also shown normalized by their own initial local maximum.

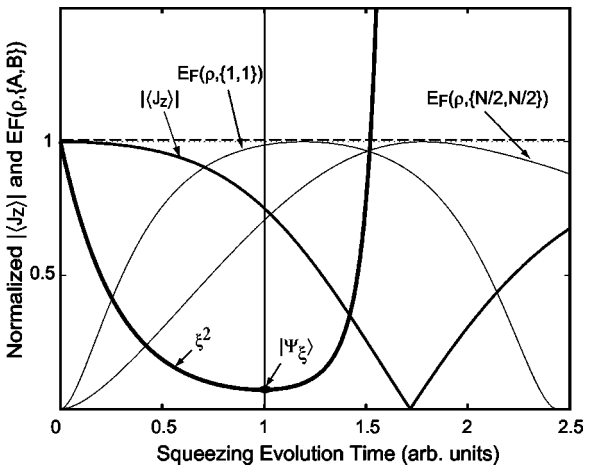

FIG. 6. Spin-squeezing evolution for a system of $N = 50$ spin-1/2 particles evolving by the countertwisting Hamiltonian as measured by the squeezing parameter ξ^2. The time is scaled such that maximal spin squeezing occurs at $t = 1$. The mean J_z and the entanglements of formation are all independently normalized by their own maximum in the time period shown. Notice that the small-scale correlations $E_F(\rho,\{1,1\})$ peak before the large-scale correlations $E_F(\rho,\{N/2,N/2\})$, as the squeezing evolves.

The small-scale entanglement $\{1,1\}$ reaches its peak before the large-scale entanglement $\{N/2,N/2\}$ does. If we analyze the relative rate of growth of the different scales of entanglement at early times, we see an intuitive ordering. Figure 7 shows the small-time logarithmic negativities (for all even splits) and the entropy of formation (for the extremal splits) normalized by their respective maxima over that interval. As the state becomes squeezed, the $\{1,1\}$ correlations form first, followed by the $\{1,2\}$, then the $\{2,2\}$, and so on, up to $\{N/2,N/2\}$. This observation suggests that small-scale correlations typically peak earlier than larger-scale correlations when evolving under quadratic Hamiltonians.

Another observation is that for small times, the state gets progressively more entangled in the sense of majorization [45]. In other words, the eigenvalues of $\mathrm{Tr}_k[\rho(t+dt)]$ are more disordered than the eigenvalues of $\mathrm{Tr}_k[\rho(t)]$ for all $k \leqslant N/2$ and small t. Thus, despite certain ordering difficulties with various entropies, the entanglement of any split is *strictly* increasing initially.

It is also important to quantitatively compare the entanglement measures for spin-squeezed states and the symmetric reference states. Figure 8(a) shows the even split entropy $E_F(|\Psi_\xi\rangle,\{N/2,N/2\})$ of the optimally squeezed state as a function of N. From a numerical fit, we find that

$$E_F(|\Psi_\xi\rangle,\{N/2,N/2\}) \approx 0.46\log_2(N) - \log_2(e). \tag{59}$$

For smaller-scale entanglement, Fig. 8(b) displays the two-spin entropy $E_F(|\Psi_\xi\rangle,\{1,1\})$. The values approach but never exceed the curve for $|\widetilde{N/2}\rangle$. Indeed, it can be shown that in the large-N limit, the two-spin concurrence scales identically

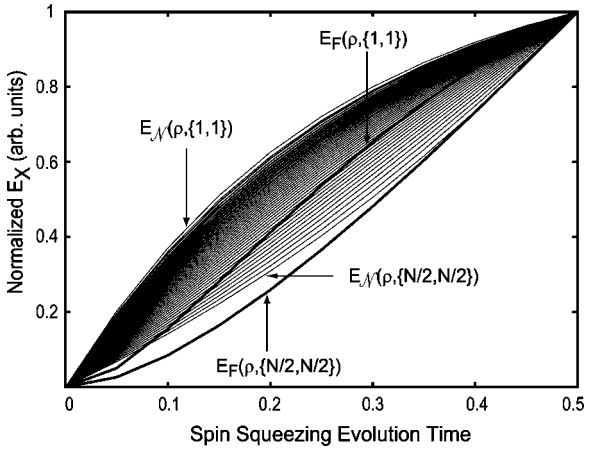

FIG. 7. Entanglement measures for a system of $N=50$ spin-1/2 particles evolving under the influence of a countertwisting spin-squeezing Hamiltonian. The time is scaled such that the squeezing parameter achieves its minimum at $t=1$ (the small-time evolution is depicted) and all entanglement measures are independently normalized by their own maximum in the time period shown. The entropy of formation, $E_F(\rho,\{A,B\})$ is shown for the extremal bipartite splits $\{1,1\}$ and $\{N/2,N/2\}$, while the logarithmic negativity $E_N(\rho,\{A,B\})$, is depicted for the partitions $\{1,1\},\{1,2\}$, $\{2,2\},\ldots,\{N/2-1,N/2\},\{N/2,N/2\}$. It can be seen that small-scale correlations tend to peak before their large-scale counterparts; the entanglement measures are strictly ordered according to the number of particles remaining N_r.

for the two states: $\mathcal{C}(|\widetilde{N/2}\rangle)\approx\mathcal{C}(|\Psi_\xi\rangle)\approx 1/N$, thus the entanglements of formation must also converge.

For a specified number of particles ($N=50$), the family of states generated by applying the countertwisting Hamiltonian to a polarized sample are displayed in the $[E_F(\rho(t),\{N/2,N/2\}),E_F(\rho(t),\{1,1\})]$ space of Fig. 8(c). Again the small-scale entanglement grows faster than the large-scale entanglement, but eventually decays to zero as the large scale entanglement takes over. The disordered nature of the countertwisting Hamiltonian dominates at long times as the value of the large-scale entanglement diffuses and the small-scale entanglement remains near zero. In contrast, the application of a twisting Hamiltonian $H_t=J_x^2$ (which, unlike the countertwisting Hamiltonian, creates squeezed states with a rotating axis of squeezing) is seen to be much more periodic. The states it generates are similar to the countertwisting states initially, but they eventually converge to the GHZ state and then return along the same trajectory.

The entropies of extremal splits ($\{1,1\}$ and $\{N/2,N/2\}$) capture much of the character of a many-particle entangled state, but there are, of course, a large number of other bipartite splits to consider. The introduction of the information contained in all other splits potentially brings up more interesting entanglement characteristics. As in Fig. 4, we can efficiently calculate all even split bipartite logarithmic negativities for large number states as they become spin squeezed. The characteristic of early small-scale entanglement being transformed into subsequent large-scale entanglement during the course of evolution is again apparent. Nonetheless, for this particular case, the intermediate splits do not provide a considerable amount of additional insight compared to that from the extremal splits.

2. Squeezing under particle loss

We now address how the spin-squeezing parameter behaves under particle loss. Given the expectation values of a set of operators on a symmetric density matrix, it is simple to determine the moments of the same state with a certain number of particles removed. If ρ_N is symmetric, so are all of its reduced density matrices ρ_{N_r}, where $1\leqslant N_r\leqslant N$. Given single-particle operators o_i, we know that

$$\mathrm{Tr}_N(o_i\cdots o_j\rho_N)=\mathrm{Tr}_{N-1}(o_i\cdots o_j\rho_{N-1}) \tag{60}$$

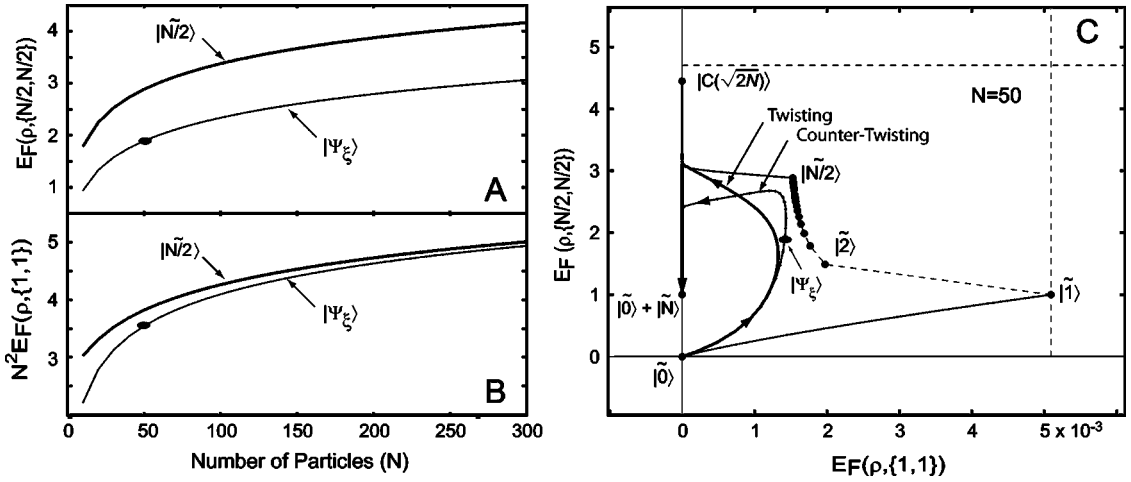

FIG. 8. (a) A plot of the even split entanglement of formation (and entropy), $E_F(\rho,\{N/2,N/2\})$, for a system of N spin-1/2 particles evolved under a countertwisting spin-squeezing Hamiltonian. The state $|\Psi_\xi\rangle$ minimizes the squeezing parameter, ξ^2. (b) A similar plot using the scaled entanglement of formation, $N^2E_F(\rho,\{1,1\})$, for a system with all but two particles removed. (c) The time evolution of states evolving under both the countertwisting Hamiltonian $[H_{ct}=(J_+^2-J_-^2)/i]$ and twisting Hamiltonian $(H_t=J_x^2)$ in the space of extremal split entanglement.

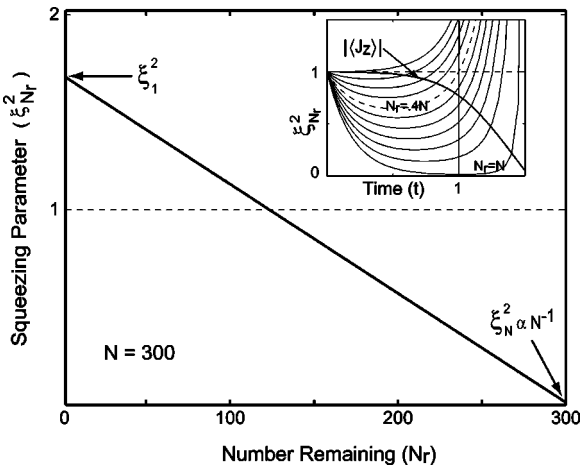

FIG. 9. Spin-squeezing reduction due to particle loss for a system initially containing $N=300$ spin-1/2 particles. The lower right corner of the plot reflects the minimum value of the squeezing parameter ξ^2 achieved via a countertwisting Hamiltonian. As particles are removed from the optimally squeezed system, the value of $\xi^2_{N_r}$ moves up and left along the plotted line, eventually crossing unity for finite number systems. The inset shows the time evolution of ξ^2 for different numbers of remaining particles, N_r.

assuming the indices of the operators are not the ones traced out. With this observation and the fact that for symmetric states

$$\langle J_z\rangle_N = N\mathrm{Tr}_N(j_{z,i}\rho_N) \tag{61}$$

and

$$\langle J_z\rangle_{N-1} = (N-1)\mathrm{Tr}_{N-1}(j_{z,i}\rho_{N-1}), \tag{62}$$

we find

$$\langle J_z\rangle_{N-1} = \frac{N-1}{N}\langle J_z\rangle_N . \tag{63}$$

Similarly, it is easy to show

$$\langle J_x^2\rangle_{N-1} = \frac{N-2}{N}\langle J_x^2\rangle_N + \frac{1}{4}. \tag{64}$$

Using these relations and taking the large-N limit, we find that the spin-squeezing parameter of a state with N_r spins remaining ($\xi^2_{N_r}$) is dependent on the initial squeezing parameter (ξ^2_N) and polarization of the state with all spins remaining in the following way:

$$\xi^2_{N_r} = \xi^2_1 + (\xi^2_N - \xi^2_1)\frac{N_r - 1}{N-1} \tag{65}$$

where $\xi^2_1 \equiv N^2/(4\langle J_z\rangle^2_N)$.

The inset of Fig. 9 shows the spin-squeezing behavior for $N=300$ as a function of time. Considering only the time when the state of all the spins is maximally squeezed ($t=1$), we plot the spin squeezing parameter as a function of number remaining in Fig. 9, which behaves according to Eq. (65). For this finite number case, the spin-squeezing is lost after some fraction of the spins are removed. As N goes to infinity though, $\langle J_z\rangle_N \to N/2$ ($\xi_1 \to 1$) and $\xi_N \to 0$, so all spins need to be removed for the state to completely lose its spin squeezed character.

In a similar analysis, Simon and Kempe [15] have shown that spin-squeezed states remain squeezed until more than 29% of the particles have *depolarized*. Thus spin-squeezed states are robust to both particle loss and dephasing with constant N. (See Refs. [9,16] for a more complete treatment of how the spin-squeezing parameter behaves under continuous generation and decoherence.) However, robustness to particle loss and dephasing do not necessarily imply on each other because the GHZ states are remarkably robust to local depolarization [15], but, obviously, maximally fragile under particle loss. The complete relationship between robustness to particle loss and dephasing is an interesting direction for further research.

B. Generating entangled states

Instead of characterizing what states a particular process produces, consider the reverse problem of determining the process necessary to generate a desired state from an initially separable state. The completely polarized initial state ($|\tilde{0}\rangle$ or $|\tilde{N}\rangle$) is usually chosen, both because it is completely separable at all levels and it is easily prepared in the lab (e.g. via optical pumping).

It can be shown that given such a state and access to Hamiltonians of the form J_x, J_y, J_z, and J_x^2, i.e., the generators are all rotations plus a single nonlinearity, one can produce *any* symmetric state by an algorithm that switches between the Hamiltonians in time [46]. Unfortunately, proving this statement does not necessarily lead to the most efficient way to create a particular state. Knowing which states are prohibitively expensive to produce is an important experimental question. An interesting, but difficult, way to characterize a state is by quantifying the resources needed to create that state, given a certain set of generators. For example, one could define a cost metric which is a function of how many times the Hamiltonians must be switched and the length of time necessary to produce a particular state.

Of course, all these issues are context specific, but we can summarize certain results. Simply observing what the application of a particular Hamiltonian produces is a first step. The countertwisting Hamiltonian presented earlier produces optimal squeezing but does not produce any recognizable reference state (since the dynamics for large N becomes highly disordered for long times). A one-axis twisting Hamiltonian of J_x^2 produces some squeezing which does not scale optimally [2]. However, the time dependence of the entanglement produced by this Hamiltonian is much more periodic and ordered than the countertwisting version. In fact, it produces the GHZ state halfway through its period as is indicated in Fig. 8(c). Mølmer and Sørensen [47] have proposed a robust scheme for generating the GHZ state of many hot ions taking advantage of this effect.

Unanyan *et al.* have shown that by using adiabatic passage and energy-level navigation methods one can produce

the GHZ state and all $|\tilde{m}\rangle$ states [48]. However, it remains unclear what the most efficient method is to generate these states, or the bipartite entropy maximizing states presented here, in the asymptotic limit of large N.

VI. CONCLUSION

In this paper, we analyzed the microscopic structure of entanglement and its robustness to particle-loss for many-particle symmetric states. Our approach proceeded by comparing the features of dynamically generated squeezed states to a collection of symmetric representative states, including the GHZ and Dicke states, as well as random states and a family that we define. In order to perform the analysis, we selected several bipartite entanglement measures: the reduced entropy of entanglement, the entanglement of formation, and the logarithmic negativity. By computing these bipartite measures for all possible reductions and partitions of the systems, we were able to construct a picture of multiscale entanglement.

Our analysis benefitted from simulations of many-particle systems. The computational results helped to bolster physical insight and provide a starting point for analytically treating the asymptotic scaling of various entanglement measures. In order to circumvent the exponential scaling of the density matrix for arbitrary N-particle states, we restricted our analysis to the symmetric subspace. In Sec. III, we developed machinery for computing the above entanglement monotones for symmetric states in a computationally efficient manner. As a result, our simulations were capable of handling systems with $N\sim 10^3$ particles without making any dynamical approximations.

In Sec. IV, we characterized the entanglement of the representative states in detail, focusing on the trade-off between those states that maximize the entanglement measures and those that are robust under particle loss. We also analyzed several important ordering issues between the different measures. A key point we stress is that fragility is not necessarily a property of highly entangled states. With the analysis in Sec. IV, it was possible to address the evolution of microscopic entanglement in dynamically generated spin-squeezed states. Hopefully, this work helps to clarify the otherwise vague statement that ''spin-squeezed states are massively entangled.''

From this work, we anticipate several future directions. First, we plan to consider less restrictive symmetry classes, particularly the symmetry of Eq. (15). This symmetry is preserved during the unconditional evolution of an ensemble under a uniform symmetry-preserving Hamiltonian and local dephasing. For certain cases, where the emission from the particles does not physically distinguish different particles, the symmetry may also be preserved under conditional evolution. In order to perform such an analysis, it will be necessary to exploit the commutant algebra and representation theory of the permutation group [49]. A preliminary investigation suggests that it will be possible to treat the full permutation group in a manner that scales polynomially, rather than exponentially, with the number of particles.

A more straightforward objective is to generalize the treatment of this paper to particles with more than two levels. For example, we would like to describe the entanglement within an ensemble of cesium atoms, where each atom can occupy the nine magnetic sublevels of the $F=4$ ground state.

Regarding dynamically generated states, it is possible to further simplify the description of entanglement at small times. For any initially polarized state experiencing a quadratic Hamiltonian, the state and relevant entanglement measures can be described in terms of the Gaussian moments alone for short times. Deriving the exact form of this low-dimensional parametrization of entanglement measures is of experimental interest.

Finally, an important challenge is to develop techniques for efficiently generating the reference states discussed in this paper, including those with near-maximal entanglement, such as the comb states. Here, we hope to stress that theoretical treatments of many-particle spin systems are most beneficial when they adopt methods that can be experimentally implemented.

ACKNOWLEDGMENTS

The authors acknowledge a number of important discussions with Guifre Vidal, Dave Bacon, and Patrick Hayden. This work was supported in part by the DoD Multidisciplinary University Research Initiative (MURI) program administered by the Army Research Office under Grant No. DAAD19-00-1-0374 and the Caltech Institute for Quantum Information sponsored by the National Science Foundation under Grant No. EIA-0086038. J.K.S. acknowledges financial support from Hertz Foundation.

APPENDIX: SYMMETRIC STATE ENTROPY SCALING

Proposition 1. There exists a lower bound for the maximum attainable symmetric state entropy that asymptotically scales as the maximum entropy for states in $\mathbb{S}_{N/2}\otimes\mathbb{S}_{N/2}$,

$$\exists|\Psi\rangle\in\mathbb{S}_N,\delta>0,N^*>0:\forall N>N^*,$$

$$\log_2(N/2+1)-E(|\Psi\rangle,\{A,B\})<\delta. \tag{A1}$$

Proof. The proof proceeds by constructing a symmetric state, whose even split reduced entropy $E(|\Psi\rangle,\{N/2,N/2\})$ can be expressed as the asymptotic series, $\log_2(N/2+1)+\delta$. In order to obtain this series, we express the entropy in terms of the Schmidt coefficients from Eq. (42) by employing Stirling's formula. Computing the residuals that are incurred by Stirling's approximation, we obtain a bound for δ and demonstrate that it is asymptotically constant in N, i.e., $\delta\sim O(1)$.

Consider the family of $|C(s)\rangle$ states, defined in Sec. IV A 3, whose Schmidt decomposition, according to Eq. (42), is given by

$$|C(s)\rangle=A\sum_{m=-N/s}^{N/s}\sum_{i=0}^{N-k}\sum_{j=0}^{k}\frac{C_{N,m}\delta^N_{\frac{2}{2}+ms,i+j}}{C_{N-k,i}C_{k,j}}|\tilde{i}\rangle_{N-k}|\tilde{j}\rangle_k, \tag{A2}$$

where $A=\sqrt{2s/N}$. We wish to choose the value of s in $|C(s)\rangle$ such that the matrix c becomes block diagonal in the large-N limit, which will happen provided that the $|\tilde{m}\rangle$ contributing to $|C(s)\rangle$ are sufficiently separated. For an orthogonal Schmidt matrix, Eq. (13) can be solved in a closed form and the total entropy is a weighted sum of the entropies contributed by each participating, $|\tilde{m}\rangle$.

The required separation between nonzero $|\tilde{m}\rangle$ in $|C(s)\rangle$ as well as their contributing entropies can be found by considering $c_m(i)$, the c_{ij} matrix elements as a function of i for a given value of m. This leads to the distribution

$$c_m(i)=\sqrt{\frac{\binom{N-k}{i}\binom{k}{m-i}}{\binom{N}{m}}}, \tag{A3}$$

which can be approximated using Stirling's formula,

$$\ln n!=n\ln n-n+\sqrt{2\pi n}+\frac{1}{12n}+O(n^{-2}), \tag{A4}$$

to obtain the expression

$$c_m^2(i)=2^{-(m+1/2)}\exp\left[\frac{i^2-i+m+m^2}{12i^2m-12im^2}\right]i^{-(i+1/2)}m^{m+1/2} \times(m-i)^{i-m-1/2}\pi^{-1/2}+O(m^{-2}) \tag{A5}$$

for $c_m^2(i)$ as $N\to\infty$. The residual terms are of order m^{-2}.

Unfortunately, it is not known how to evaluate the entropy of Eq. (A5) because the discrete sum

$$S(m)=-\sum_{i=0}^{\infty}c_m^2(i)\log_2 c_m^2(i) \tag{A6}$$

cannot be expressed in closed form. However, the moments of $c_m(i)$ can be computed analytically:

$$\overline{i}=\langle i\rangle=\frac{m}{2}, \tag{A7}$$

$$\sigma^2=\langle i^2\rangle-\langle i\rangle^2=\tfrac{1}{12}m(m+2), \tag{A8}$$

and it can be seen that all higher cumulants vanish in the large-N limit.

The entropy contributed by each $|\tilde{m}\rangle$ in $|C(s)\rangle$ when m is large can be computed by approximating the $c_m^2(i)$ as Gaussian,

$$c_m^2(i)=\sqrt{\frac{1}{m\pi}}\exp\left[\frac{-1}{4m}-\frac{\sqrt{3}(i-m/2)^2}{\sqrt{m(m+2)}}\right]+O(m^{-2}), \tag{A9}$$

and transforming the summation in Eq. (A6) into an integral

$$S_m-\epsilon=-\int_0^{\infty}c_m^2(i)\log_2 c_m^2(i)di+\int O(m^{-2})di, \tag{A10}$$

where the error term ϵ must be obtained using the Abel-Plana procedure [50] for computing the difference between a discrete sum and its corresponding integral. An upper bound for the integral over the residual $O(m^{-2})$ terms can be found to converge to $\varepsilon=\sqrt{2\pi}m^{-2}\exp(-m^2)/128$, by considering the asymptotic series of the Γ function [51].

The resulting entropy, in the large-m limit, with the Abel-Plana corrections and the error bounds from higher-order Stirling terms can be shown to have the form

$$S_m=\frac{e^{-1/4m}m^{1/4}(2+m)^{3/4}}{3^{1/4}\sqrt{2m(2+m)}\ln 2}+\vartheta_3(0,m^{-1/2}e^{-1/4m}) -\frac{1}{2}\vartheta_4(0,1/\sqrt{\pi})+\varepsilon, \tag{A11}$$

where $\vartheta_n(u,v)$ is the elliptic theta function of order n [51]. Computing the entropy of the full state requires evaluating the discrete sum over m. We chose the comb spacing to be $s=\sqrt{2N}$ based on Eq. (A8). Performing the final sum leads to

$$E(|\Psi\rangle,\{N/2,N/2\})=\left(1+\frac{1}{2\sqrt{N}}\right)\log_2 N+O(Ne^{-\sqrt{N}})+\varepsilon, \tag{A12}$$

where the first residual term reflects the finite overlap of the $c_m^2(i)$, i.e., corrections that arise because **c** is not perfectly block diagonal.

Finally, it is possible to express the reduced entropy as an asymptotic series

$$E(|\Psi\rangle,\{N/2,N/2\})\to\log_2(N/2+1)-O(1), \tag{A13}$$

which completes the proof.

[1] W. Dür and J.I. Cirac, Phys. Rev. A **61**, 042314 (2000).
[2] M. Kitagawa and M. Ueda, Phys. Rev. A **47**, 5138 (1993).
[3] A. Kuzmich, L. Mandel, and N.P. Bigelow, Phys. Rev. Lett. **85**, 1594 (2000).
[4] J. Hald, J.L. Sørensen, C. Schori, and E.S. Polzik, Phys. Rev. Lett. **83**, 1319 (1999).
[5] V. Meyer, M.A. Rowe, D. Kielpinski, C.A. Sackett, W.M. Itano, C. Monroe, and D.J. Wineland, Phys. Rev. Lett. **86**, 5870 (2001).
[6] D.J. Wineland, J.J. Bollinger, W.M. Itano, and D.J. Heinzen, Phys. Rev. A **50**, 67 (1994).
[7] B. Julsgaard, A. Kozhekin, and E.S. Polzik, Nature (London) **413**, 400 (2001).
[8] L.K. Thomsen, S. Mancini, and H.M. Wiseman, Phys. Rev. A **65**, 061801 (2002).
[9] D. Ulam-Orgikh and M. Kitagawa, Phys. Rev. A **64**, 052106 (2001).
[10] X. Wang and K. Mølmer, Eur. Phys. J. D **18**, 385 (2002).

[11] A. Sørensen, L.-M. Duan, J. Cirac, and P. Zoller, Nature (London) **409**, 63 (2001).
[12] A.S. Sørensen and K. Mølmer, Phys. Rev. Lett. **86**, 4431 (2001).
[13] W. Dür, Phys. Rev. A **63**, 020303 (2001).
[14] A.K. Rajagopal and R.W. Rendell, Phys. Rev. A **65**, 032328 (2002).
[15] C. Simon and J. Kempe, Phys. Rev. A **65**, 052327 (2002).
[16] A. André and M.D. Lukin, Phys. Rev. A **65**, 053819 (2002).
[17] A. Wong and N. Christensen, Phys. Rev. A **63**, 044301 (2001).
[18] K.G.H. Vollbrecht and R.F. Werner, Phys. Rev. A **64**, 062307 (2001).
[19] N. Gisin and H. Bechmann-Pasquinucci, Phys. Lett. A **246**, 1 (1998).
[20] G. Vidal, e-print quant-ph/9807077.
[21] M. Horodecki, P. Horodecki, and R. Horodecki, Phys. Rev. Lett. **84**, 2014 (2000).
[22] T. Wei, K. Nemoto, P. Goldbart, P. Kwiat, W. Munro, and F. Verstraete, e-print quant-ph/0208138.
[23] S. Hill and W.K. Wootters, Phys. Rev. Lett. **78**, 5022 (1997).
[24] W.K. Wootters, Phys. Rev. Lett. **80**, 2245 (1998).
[25] C.H. Bennett, G. Brassard, S. Popescu, B. Schumacher, J.A. Smolin, and W.K. Wootters, Phys. Rev. Lett. **76**, 722 (1996).
[26] C.H. Bennett, D.P. DiVincenzo, J.A. Smolin, and W.K. Wootters, Phys. Rev. A **54**, 3824 (1996).
[27] G. Vidal and R.F. Werner, Phys. Rev. A **65**, 032314 (2002).
[28] W. Dür, J.I. Cirac, M. Lewenstein, and D. Bruss, Phys. Rev. A **61**, 062313 (2000).
[29] D.P. DiVincenzo, P.W. Shor, J.A. Smolin, B.M. Terhal, and A.V. Thapliyal, Phys. Rev. A **61**, 062312 (2000).
[30] M. Horodecki, P. Horodecki, and R. Horodecki, Phys. Rev. Lett. **80**, 5239 (1998).
[31] M. A. Nielsen and I.L. Chuang, *Quantum Computation and Quantum Information* (Cambridge University, Cambridge, 2000).
[32] R. Paškauskas and L. You, Phys. Rev. A **64**, 042301 (2001).
[33] G. Vidal, Phys. Rev. Lett. **83**, 1046 (1999).
[34] J. Eisert and H.J. Briegel, Phys. Rev. A **64**, 022306 (2001).
[35] D.M. Greenberger, M. Horne, and A. Zeilinger, *Bell's Theorem, Quantum Theory, and Conceptions of the Universe* (Kluwer, Dordrecht, 1989), p. 69.
[36] V. Coffman, J. Kundu, and W.K. Wootters, Phys. Rev. A **61**, 052306 (2000).
[37] W. Dür, G. Vidal, and J.I. Cirac, Phys. Rev. A **62**, 062314 (2000).
[38] M. Koashi, V. Buzek, and N. Imoto, Phys. Rev. A **62**, 050302 (2000).
[39] F. Verstraete, J. Dehaene, B.D. Moor, and H. Verschelde, Phys. Rev. A **65**, 052112 (2002).
[40] C.H. Bennett, S. Popescu, D. Rohrlich, J.A. Smolin, and A.V. Thapliyal, Phys. Rev. A **63**, 012307 (2000).
[41] A. Acín, G. Vidal, and J.I. Cirac, e-print quant-ph/0202056.
[42] M. Ohya and D. Petz, *Quantum Entropy and Its Use* (Springer-Verlag, Berlin, 1993), Chap. 15.
[43] G. Vidal (private communication).
[44] K. Życzkowski, P. Horodecki, M. Horodecki, and R. Horodecki, Phys. Rev. A **65**, 012101 (2001).
[45] M.A. Nielsen, Phys. Rev. Lett. **83**, 436 (1999).
[46] D. Bacon and L. Viola (private communication).
[47] K. Mølmer and A. Sørensen, Phys. Rev. Lett. **82**, 1835 (1999).
[48] R.G. Unanyan, M. Fleischhauer, N.V. Vitanov, and K. Bergmann, e-print quant-ph/0205118.
[49] B. E. Sagan, *The Symmetric Group*, 2nd ed., Graduate Texts in Mathematics Vol. 203 (Springer-Verlag, New York, 2001).
[50] G. Hardy, *Divergent Series* (Chelsea, New York, 1991).
[51] *Handbook of Mathematical Functions*, edited by M. Abramowitz and A. Stegun (Dover, New York, 1972).
[52] We work with the convention that for any bipartite split of a system, $\{A,B\}$, the symbol A is equivalent to a list of the particles residing on its side of the split, and likewise for B. N_A and N_B are the number of particles on each side of the split; d_A and d_B are the Hilbert space dimensions of each side, generally 2^{N_A} and 2^{N_B} for nonsymmetric collections of spin-1/2 particles.
[53] We use the convention that for any bipartite measure X if $j+k$ is less than the number of spins N in $|\Psi\rangle$, the possibly mixed state that the measure $E_X(|\Psi\rangle,\{j,k\})$ should act on is actually $\mathrm{Tr}_{N-j-k}|\Psi\rangle\langle\Psi|$. For the concurrence, we use the similar convention $\mathcal{C}(|\Psi\rangle)=\mathcal{C}(\mathrm{Tr}_{N-2}|\Psi\rangle\langle\Psi|)$.